Laser and Particle Beams

cambridge.org/lpb

High-intensity pulsed ion beam composition and the energy spectrum using the time-of-flight method

A. I. Pushkarev, Y. I. Isakova and A. I. Prima

Tomsk Polytechnic University, 30, Lenin Ave 634050, Tomsk, Russia

Research Article

Cite this article: Pushkarev AI, Isakova YI, Prima AI (2018). High-intensity pulsed ion beam composition and the energy spectrum using the time-of-flight method. *Laser and Particle Beams* **36**, 210–218. https://doi.org/10.1017/S0263034618000186

Received: 19 April 2018
Accepted: 27 May 2018

Key words:
Energy spectrum; Faraday cups; high-intensity pulsed ion beam composition; magnetically insulated diodes; time-of-flight

Author for correspondence:
Y. I. Isakova, Tomsk Polytechnic University, 30, Lenin Ave 634050, Tomsk, Russia. E-mail: isakova_yulia@tpu.ru

Abstract

The paper describes a technique for operative control of the high-intensity pulsed ion beam parameters. The time-of-flight diagnostics uses one high-speed Faraday cup sensor with magnetic cut-off of low-energy electrons. The technique makes it possible to determine the composition of the beam (the type of ions and the degree of ionization), the absolute values of the current density of ions and the energy spectrum for each type of ions with an error of <±10%. The technique was tested at different pulsed ion accelerators and ion diodes both with self-magnetic insulation (accelerating voltage of 200–250 kV, ion current density of 20–300 A/cm^2) and external magnetic insulation of the electrons (400–500 kV, 200 A/cm^2). The article presents a comparative analysis of two types of Faraday cups with magnetic cut-off of the electrons and with electric bias.

Introduction

Improvement in the production of mechanical engineering products is hampered without the use of new progressive technological processes that enhance the operational lifetime and reliability of components in the most severe operating conditions. In this regard, the methods for surface hardening by laser irradiation, electron and ion beams attract a lot of attention (Proskurovsky *et al.*, 2000; Bocharov *et al.*, 2018). The exposure of a high-intensity pulsed ion beam (HIPIB) at gigawatt power level with the energy density of 2–10 J/cm^2 provides a rapid heating of the surface layer at a rate of 10^9 K/s, followed by a fast cooling at a speed of 10^8–10^{10} K/s (Bystriskii and Didenko, 1989). Such treatment of an item makes it possible to obtain in the surface layers compositions and nanoscale structures that are inaccessible to any of the traditional metallurgical methods. As a result, the properties of materials are improved: hardness, strength, wear and corrosion resistance, etc.

The HIPIB composition determines the depth of a modified layer of a treated item and the specific energy release. Therefore, optimizing of the treatment procedure requires to control the composition and the quantitative ratio of the ions in the beam. In metals and alloys with a range of ions (ion energy of 200–300 keV) of <0.5 μm, the thermal front propagates toward the end of the pulse to a depth of 2–4 μm (Pushkarev *et al.*, 2015a). Therefore, for metal products, the composition of HIPIB is not as important as the depth of propagation of the thermal front. However, for a study and optimization of the ion diode operation, it is important to know the composition of the ion beam.

A method for measuring the composition of an ion beam with the acceleration of ions in an electric field and their spatial separation by means of a magnetic field was first proposed by J. Tomson in 1913. In 1920, Aston designed a prototype of a modern magnetostatic mass spectrometer (Aston, 1920). To detect ions with a large mass in a Thomson spectrometer, it was necessary to use a magnetic field with an induction of more than 1 T, which complicates the instrument and increases its dimensions and mass. Detailed information on the composition of the beam, the energy spread of ions in the Thomson spectrometer is obtained using the track diagnostics based on CR-39 plastics (Fleischer *et al.*, 1965; Cartwright *et al.*, 1978). However, processing of the recording plates requires a lot of time and does not allow for a quick monitoring of the beam parameters. The use of photosensitive semiconductor matrices in the Thomson spectrometer (Kasuya *et al.*, 1999) (for recording the spatial separation of ions) is difficult due to destruction of the photosensitive elements in high-voltage sources of HIPIB with a large energy density.

To analyze the HIPIB composition, a phenomenon of spatial separation of different types of ions along the path from the diode to the recording device can be used. When accelerating in the anode–cathode (A–C) gap of the diode, ions of different mass and degree of ionization acquire the same energy, but different speeds. The idea of the time-of-flight mass analyzer belongs to Stephens, who proposed the design of the device in 1946 (Stephens, 1946). The first analyzer was constructed by Wiley and MacLaren (1955). The advantages of time-of-flight

© Cambridge University Press 2018

CAMBRIDGE UNIVERSITY PRESS

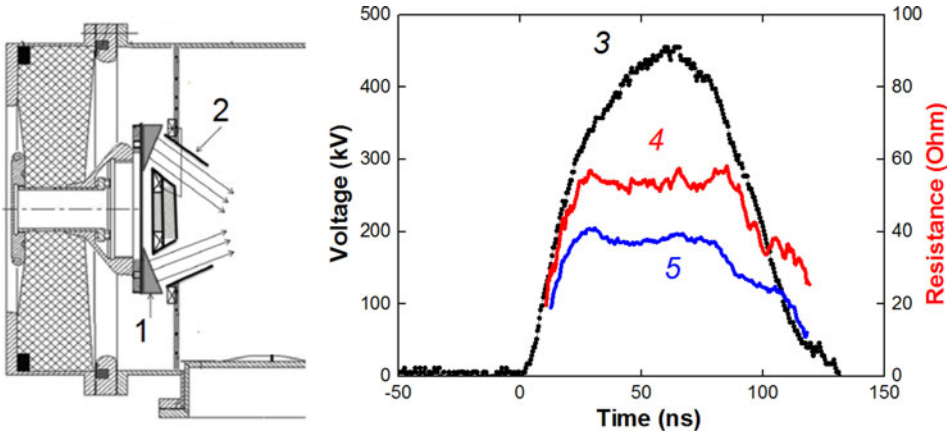


Fig. 1. Diagram of the diode assembly of the BIPPAB-450 accelerator (1 – anode, 2 – cone cathode), waveforms of voltage (3) and calculated resistance of a load (4–53, 5–38 Ω).

mass analyzers include the high upper threshold of the detected ion mass, limited only by the decrease in the sensitivity of the ion detector. The composition of HIPIB is determined by a time-of-flight method using two ion current sensors placed at different distances downstream from the diode (Moskalev, 1992). A more detailed review on the history of development of time-of-flight mass spectrometers from the moment of their invention to the present time can be found in Mamyrin (2001).

The use of a high-speed recording device (an ion collector) and a wideband oscilloscope allows the ion beam to be monitored quickly using only one sensor installed at a sufficient distance from the diode. The purpose of this work is the development and testing of a high-resolution time-of-flight technique for operational control of HIPIB composition and the energy spectrum.

Ion beam composition measurement procedure

To analyze HIPIB composition, we used the time-of-flight diagnostics with a collimated Faraday cup (CFC) (Ghadikolaee and Ghadikolaee, 2012) with magnetic cut-off as a recording device for ions. It was assumed that in the diode, different ions are accelerated synchronously during the accelerating voltage pulse; the concentration of the anode plasma does not limit the ion current density; in the ion drift path from the diode to the CFC, their velocity does not change. The density of the ion beam usually does not exceed 10^{12} cm^{-3}, so the probability of ion collisions (and changes of their velocity) in the drift region is negligible.

The signal at the CFC is delayed due to the time required for ions to travel from the diode to the device. The delay is

$$\Delta t = \frac{D}{v_\mathrm{i}}, \tag{1}$$

where D is the distance from the CFC to the diode, v_i = const is the ion velocity in the drift region.

As an ion passes through the A–C gap, it acquires kinetic energy equal to

$$E = \frac{m_\mathrm{i} \times v_\mathrm{i}^2}{2} = z \times U, \tag{2}$$

where m_i and z are the mass and charge of an ion, respectively, and U is the accelerating voltage.

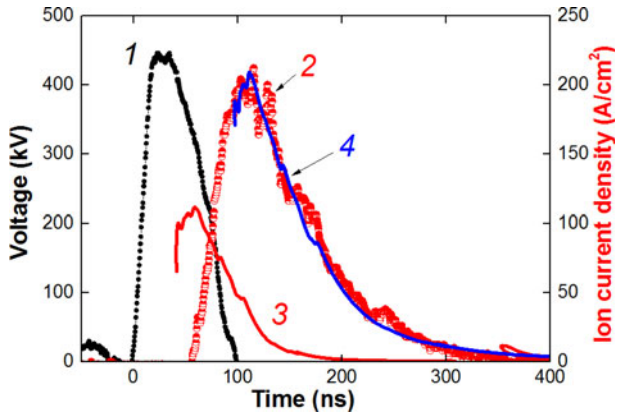


Fig. 2. Waveforms of voltage (1) and ion current density (2, points). Curve 3 is the calculated current density of protons; curve 4 is the calculated current density of C^+.

From Eqs. (1) and (2), we obtain an equation for calculating the arrival delay of ions to the CFC:

$$\Delta t = D\left(\frac{m_\mathrm{i}}{2zU}\right)^{1/2}. \tag{3}$$

In the space-charge limitation regime and in non-relativistic approximation, taking into account the plasma expansion across A–C gap, the ion current density in the diode is described by (Langmuir, 1913)

$$j(t) = \frac{4K\varepsilon_0\sqrt{(2z)}}{9\sqrt{m_\mathrm{i}}} \times \frac{U^{3/2}}{(d_0 - vt)^2}, \tag{4}$$

where d_0 is the initial A–C gap spacing, ε_0 is the absolute permittivity, v is the plasma expansion velocity, and K is the ion current amplification coefficient.

Equations (3) and (4) were used to model the signal profile from the CFC. For each instant of the voltage applied to the diode (0.4 ns step), we calculated the current density of a certain type of ions and the delay in the arrival of these ions to the CFC. The calculated curves were compared with the experimental data. Such a technique allows for a more accurate determination of HIPIB composition than that described by Furman *et al.* (2007). The plasma expansion velocity (1.2–1.6 cm/μs) was determined from the diode impedance by a method described by Pushkarev *et al.* (2014).

https://doi.org/10.1017/S0263034618000186 Published online by Cambridge University Press

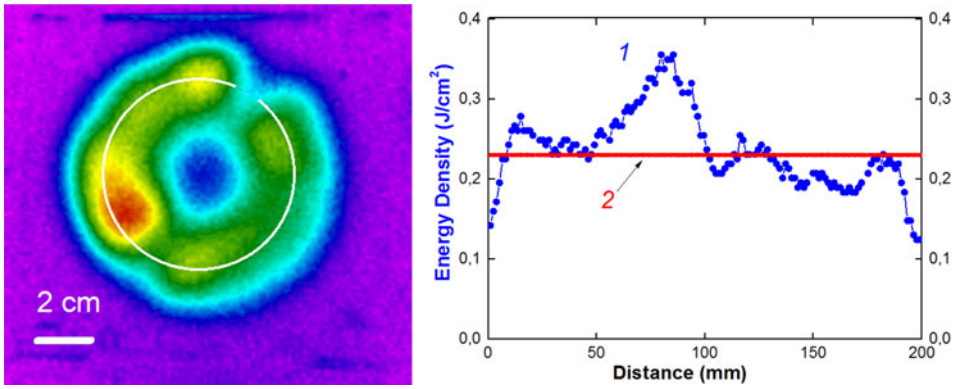


Fig. 3. Infrared image of the beam on the target, distribution of the beam energy density over the circle (1) and calculated energy density of C^+ ions (2).

Time-of-flight diagnostic testing at different diodes

A barrel diode

The time-of-flight diagnostics was used to analyze the composition of HIPIB formed by a focusing diode with a dielectric anode and radial external magnetic field (barrel diode) at the BIPPAB-450 accelerator (Xiao *et al.*, 2015; Yu *et al.*, 2017). The accelerator consists of a capacitor storage, a pulsed transformer, and a double forming line (DFL). The output of the DFL is terminated with a step-up transformer, which increases the output of the generator by up to 35 Ω. Figure 1 shows a schematic drawing of the diode connection and characteristic waveforms of the accelerating voltage when operating on a resistive load of 38 or 53 Ω. When generating an ion beam, the diode impedance was matched to the output resistances of the transformer by changing the A–C gap spacing.

The diode consists of an annular anode and two annular cathodes. The anode is made of a highly conductive material (aluminum) and has radii of 93 mm (external) and 70 mm (internal) and a surface area of 80 cm^2. The working surface of the anode contains annular grooves, which are filled with polyethylene. The cathodes are made from stainless steel. The barrel design of the diode provides a closed electrons drift in the A–C gap (Humphries, 1990). The formation of the anode plasma occurs during the breakdown on the dielectric coating surface on the anode ($B > B_{cr}$) or during ionization of the anode surface by accelerated electrons ($B \sim B_{cr}$) (Pushkarev *et al.*, 2015a). Background pressure in the vacuum chamber was 0.01–0.03 Pa.

The voltage at the output of the accelerator was measured using a voltage divider that was installed in the transition chamber between the step-up transformer and the diode. The current at the output was measured using a Rogowski coil. The ion current density was determined by a CFC with magnetic cut-off of electrons ($B = 0.4$ T). Electric signals from the sensors were recorded with a Tektronix 2024B oscilloscope (200 MHz, 5×10^9 readings/s). The synchronization error of electrical signals did not exceed 1 ns. The calibration of the diagnostic equipment showed that it correctly reflects the operation of the accelerator in the short-circuit mode and when operating on a resistive load of 35–55 Ω (voltage 400–450 kV). The accuracy of measurement of voltage, total current of the diode, ion current density, and the frequency characteristics of the diagnostic equipment allows us to calculate the impedance of the diode and the parameters of the ion current with an error of not worse than ±10%.

In the first set of experiments, the A–C gap spacing was 6.8 mm, the magnetic induction was 0.6 T at a critical magnetic induction of 0.30–0.32 T. It is found that the ion beam formed by the barrel diode at $B > B_{cr}$ is mainly composed of C^+ carbon ions (see Fig. 2).

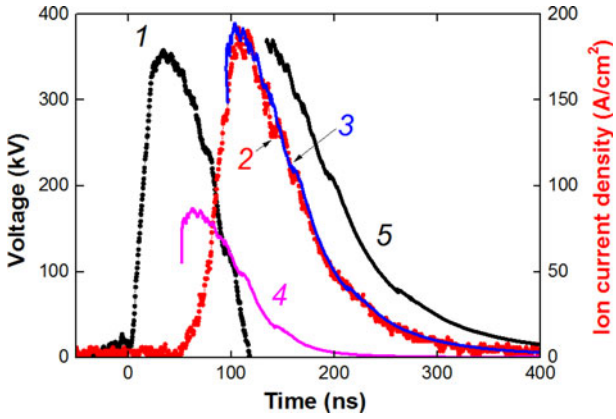


Fig. 4. Waveforms of voltage (1) and ion current density (2, points). Curve 3 is the calculated current density of C^{2+} ions; curve 4 is the calculated current density for protons; curve 5 is the calculated current density of C^+.

Measurement of the ion current density was carried out with the CFC, installed at a distance of 20 cm downstream from the diode, in the diode focus. Therefore, the ion current density calculated by Eq. (4) was increased ($K = 6$–10 for different regimes).

Time-of-flight diagnostics allows to determine the duration of anode plasma formation. Calculation of the proton current density was made for the beginning of the accelerating voltage pulse. However, the Faraday cup registered the appearance of the ion current only 10–15 ns after the plotted curve for protons (see Fig. 2). This delay corresponds to the duration of the formation of a continuous plasma layer on the anode.

The correctness of the time-of-flight diagnostics for the barrel diode was verified with the thermal imaging diagnostics (Davis *et al.*, 1997; Isakova and Pushkarev, 2018). The calculated HIPIB energy density is equal to the product of the accelerating voltage integral over the calculated ion current density (Eq. 4 at $K = 1$):

$$q_{calc}(t) = \int U(t) \times J_{ion}(t)dt = \frac{4\varepsilon_0\sqrt{2z}}{9\sqrt{m_i}} \int \frac{U^{5/2}(t)dt}{(d_0 - v \times t)^2}; \quad \text{J/cm}^2. \tag{5}$$

Figure 3 shows the thermal pattern of the beam at the target and the distribution of the energy density. The 50 μm stainless

https://doi.org/10.1017/S0263034618000186 Published online by Cambridge University Press

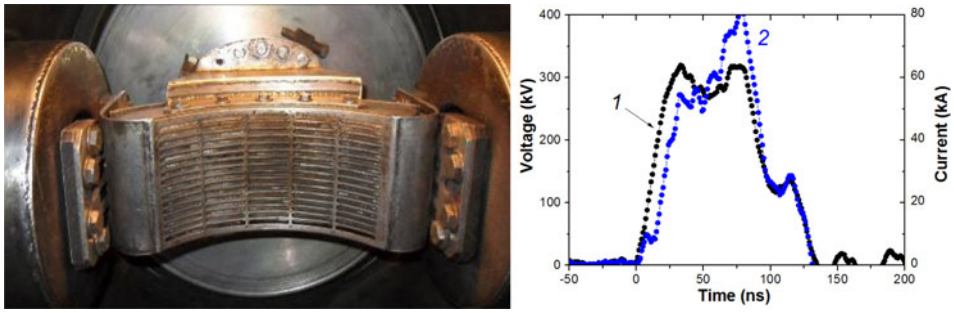


Fig. 5. A photograph of a focusing strip diode with external magnetic insulation and an open electron drift. Waveforms of the accelerating voltage (1) and total diode current (2).

steel target was placed 10 mm downstream from the cathode. Each infrared (IR) image was obtained for one accelerator shot.

The IR image of the beam was recorded through an exit window located on the flange of the diode chamber. A calcium fluoride (CaF_2) or BaF_2 parallel-sided plate was used as a window. This window features incomplete transmission in the spectral range of the IR-camera (7–14 μm); therefore, readouts of the-thermal imager that records the temperature through the window differ from the actual temperature on the target. The IR-diagnostic equipment was calibrated before the experiments (Isakova and Pushkarev, 2018 and references therein).

With a decrease in the magnetic induction in the A–C gap to a value close to the critical magnetic induction (0.34–0.37 T), the mechanism for the anode plasma formation and the composition of the ion beam changed. Figure 4 shows the results of time-of-flight diagnostics of HIPIB composition.

In this diode operation regime, in addition to an increase in the HIPIB energy density, we found an increase in the degree of ionization of carbon ions and a significant reduction in the delay time before formation of the anode plasma. In some experiments, we observed the appearance of triply ionized carbon ions. Therefore, in this mode, the formation of the anode plasma is not only due to the flashover of the anode surface coated with an insulator, but also due to the ionization of the surface material of the anode with accelerated electrons.

A low content of protons in the ion beam formed by a diode with a dielectric anode is associated with a degradation of the dielectric surface because of a prolonged operation of the diode (Zhu *et al.*, 2007). In the dielectric surface breakdown, the thermal decomposition of the organic coating of the anode and carbonization of the near-surface layer take place. The operating life of a diode with a dielectric coating does not exceed 300–400 pulses.

An ion diode with external magnetic insulation of electrons

Time-of-flight diagnostics was also tested at the TEMP-6 accelerator when operating in a single-pulse mode with a diode with a dielectric anode and external magnetic insulation of electrons (Xin *et al.*, 2011; Zhu *et al.*, 2003). The anode and cathode have a form of half cylinders to focus the HPIB. The radii of the anode and cathode were 15 and 14 cm, respectively; the slits with dimensions of 0.5 cm × 5 cm were cut out in the working part of the cathode; its transparency was 65%. A perforated polyethylene coating (holes with a diameter of 1 mm) with dimensions of 22 cm × 10 cm and a thickness of 3 mm was fixed on the working surface of the anode. To improve the generation and HIPIB-transport stability, a special cathode design was used. It was divided into two parts, one of which was placed

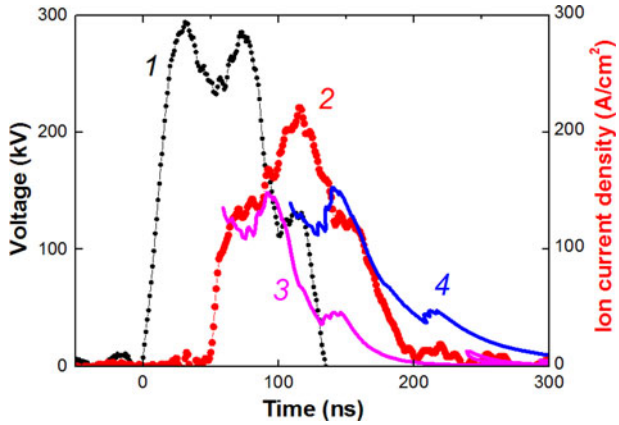


Fig. 6. Waveforms of voltage (1), ion current density (2, points). Curve 3 is the calculated current density of protons; curve 4 is the calculated current density of C^+ ions.

near the front (working) side of the anode, while the other was placed near the back side. The magnetic field was created during the current flow (100 kA, 40 μs) from the external source through the rear electrode of the cathode. This magnetic field propagated into the working A–C gap, thus providing an induction of 0.4–0.8 T. Owing to the skin effect on the cathode, the magnetic field did not penetrate into the HIPIB transport region, thus providing a forceless drift and efficient focusing of ions.

Figure 5 shows a picture of the diode and characteristic waveforms of voltage and current. In this ion diode design, an anode plasma is formed from the breakdown of the dielectric anode surface ($B > B_{cr}$).

Figure 6 shows the results of time-of-flight diagnostics of HIPIB composition.

Measurement of the ion current density was carried with the CFC, located at a distance of 15 cm downstream from the diode, in the diode focus. Therefore, the calculated values of the ion current density were increased to account for the focusing of the beam, $K_H = 7$ for protons and $K_C = 25$ for C^+ ions for the ion current density in Figure 6.

In the space-charge regime, the ion current density is [see Eq. (4)]:

$$\frac{j_H}{J_C} = \frac{\sqrt{m_C}}{\sqrt{m_H}} = \sqrt{12}. \quad (6)$$

Our investigations showed that for an ion beam formed by a dielectric diode with an external magnetic insulation, $K_C/K_H =$ 3–4; therefore, the ion beam produced by a diode in that regime contains about 50% of protons and 50% of C^+ ions.

https://doi.org/10.1017/S0263034618000186 Published online by Cambridge University Press

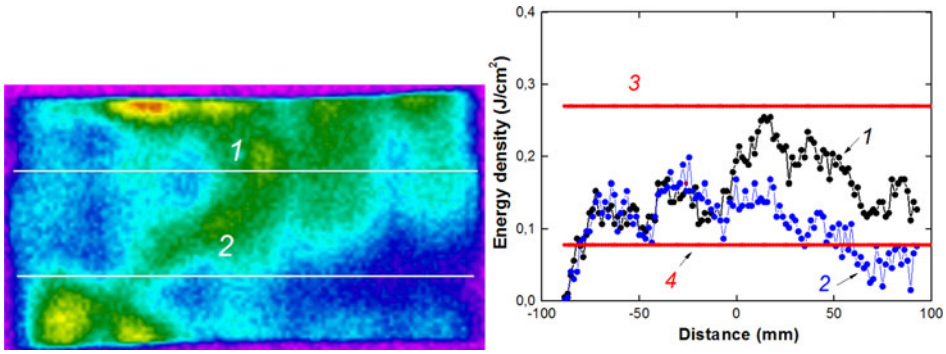


Fig. 7. HIPIB thermal imprint and the energy density distribution in the upper (1) and lower (2) horizontal sections; the calculated energy density of protons (3) and C^+ ions (4).

Figure 7 shows the results of thermal imaging diagnostics of an ion beam formed by an ion diode with a dielectric anode in the regime of external magnetic insulation (Zhu *et al.*, 2003). A stainless steel foil of 0.1 mm thick for IR image capture was placed at the output of the cathode, before HIPIB focusing.

Figure 7 also shows the calculation of the energy density of an ion beam containing protons or C^+ ions calculated from Eq. (5). The performed studies showed that the energy density of HIPIB generated by the diode in the regime of external magnetic insulation, as well as in the barrel diode agree with the calculations.

An ion diode with self-magnetic insulation of electrons

Studies on the HIPIB composition were carried out at the TEMP-4 M (Pushkarev *et al.*, 2015a) accelerator set in the mode of double pulse formation: the first negative pulse (450 ns, 150–200 kV) followed the second positive (150 ns, 200–250 kV). The ion current density on the target is 20–300 A/cm^2 for different diodes, the pulse repetition rate is 5–10 pulses/min. The accelerator consists of a capacitive storage (a pulsed voltage generator), a nanosecond pulse generator, and a vacuum diode with self-magnetic insulation of electrons. The nanosecond generator is a coaxial DFL with a liquid dielectric (water) and 4.9 Ω wave impedance. It contains the main and preliminary spark gaps. The block diagram of the diode assembly of the TEMP-4M accelerator is shown in Figure 8.

The experiments were performed with a flat diode measuring 20 cm × 4 cm. The anode is made of graphite, and the cathode is made of stainless steel with the slots of 4 mm wide and with an optical transparency of 70%. The A–C gap was selected from the condition of matching the diode impedance with the wave resistance of the DFL; it was 8–9 mm. The strip diode in the mode of self-magnetic insulation effectively works at a pressure of 0.1 Pa with a resource of more than 10^5 pulses. In the investigated diodes, an explosive electron emission (during the first pulse of negative polarity) is used to form plasma on the anode. Figure 9 shows typical waveforms characterizing the operation of a flat diode with self-magnetic insulation.

The diode current was measured by a Rogowski coil. The ion current density was measured by the CFC with magnetic cut-off of electrons ($B = 0.4$ T). The voltage at the anode was measured by a high-frequency high-voltage divider installed in front of the diode chamber. Figure 10 shows the waveforms of the accelerating voltage (second pulse) and the density of ion current generated by the planar diode with self-magnetic insulation. The distance from the diode to the CFC is 14 cm.

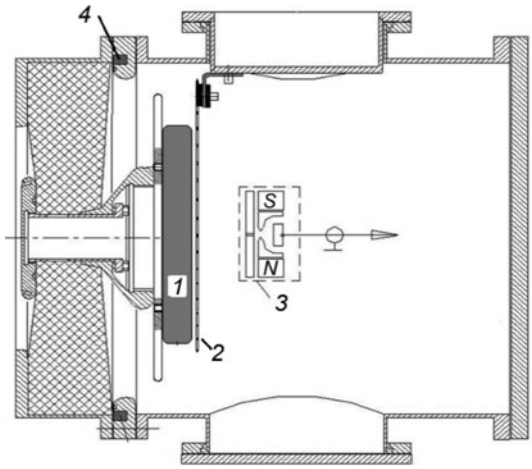


Fig. 8. Schematic representation of the diode assembly: 1 – anode, 2 – cathode, 3 – CFC, 4 – Rogowski coil.

The ion current density was calculated taking into account the plasma erosion effect when the voltage polarity at the anode changes:

$$j(t) = \frac{4K\varepsilon_0\sqrt{(2z)}}{9\sqrt{m_i}} \times \frac{U^{3/2}}{[d_0 - v(t - t_0)]^2}, \qquad (7)$$

where t_0 is the moment of polarity change at the anode (t_0 = 450 ns in Fig. 8).

The performed studies showed that HIPIB generated by a flat diode with self-magnetic insulation contains C^+ ions (80–85%) and protons. The ion current density is 5–10 times higher than the calculation in Eq. (4). An increased efficiency of ion generation is typical for diodes with self-magnetic insulation (Pushkarev *et al.*, 2015a). The amplification of the ion current density was taken into account in Figure 11 by adding the amplification coefficient K in Eq. (4), the value of which in the calculations was constant during the pulse.

With increasing the distance from the diode to the CFC, the ion current delay relative to the accelerating voltage increases. In this case, the experimental values of the ion current density and those calculated from (3) and (4) also agree well (see Fig. 11).

We observed that there is no change in the HIPIB composition (during its transport). It confirms the correctness of the time-of-flight technique for the beam compositing measurement.

The developed technique was also tested for a focusing diode with self-magnetic insulation (see Fig. 12). The distance to the CFC is 14 cm.

https://doi.org/10.1017/S0263034618000186 Published online by Cambridge University Press

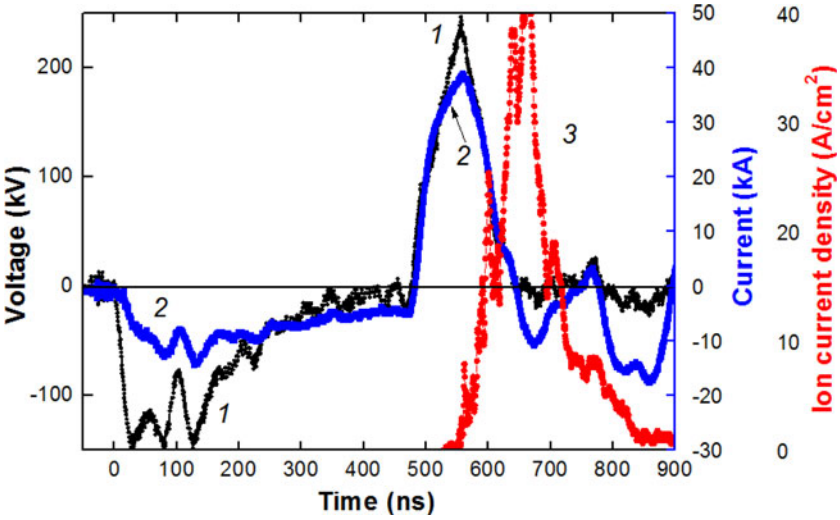


Fig. 9. Waveforms of accelerating voltage (1), total diode current (2), and ion current density (3). A–C gap spacing of 8 mm; distance to CFC is 18 cm.

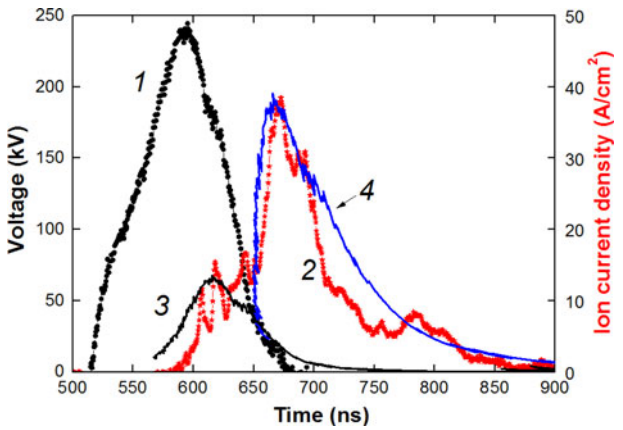


Fig. 10. Waveforms of the accelerating voltage (1) and the ion current density (2, points). Curve 3 is the calculated current density of protons; curve 4 is the calculated current density of C^+.

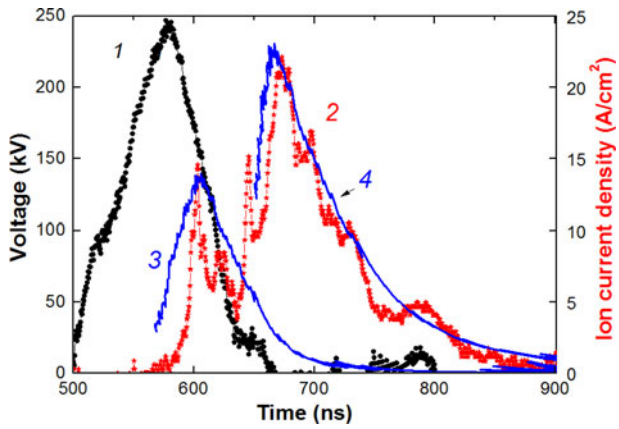


Fig. 11. Waveforms of voltage (1) and ion current density (2, points) formed by a flat diode. Curve 3 is the calculated current density of protons; curve 4 is the calculated current density of C^+ ions. Distance to CFC is 17 cm.

For the focusing diode, the main part of the ion beam is also composed of singly ionized carbon ions. The current density of C^+ ions was calculated taking into account the focusing efficiency. In the used design of the focusing diode, the ion current density was 5–8 times higher than the current density in the flat diode; the ion concentration was $(8–10) \times 10^{12}$ cm^{-3}.

Investigation of the energy distribution of ions

The energy spectrum of ions is one of the most important parameters of HIPIBs, which determines its absorption depth in a target. The developed technique allows for a quick measurement of the energy spectrum separately for each type of ions. In this case, for each value of the accelerating voltage recorded by the oscilloscope (0.4 ns step), we calculated the time delay from Eq. (3) and plotted a curve of the kinetic energy of a certain ion type synchronously with the signal from CFC. Figure 13 shows the calculated values for carbon ions generated by the flat diode (Fig. 8).

The obtained data make it possible to determine the energy distribution of ions. The energy spectrum of ions formed by the flat diode is shown in Figure 14.

The performed studies on the energy spectrum of ions formed by the planar diode with self-magnetic insulation showed that the main part of carbon and proton ions has a kinetic energy of more than 150 keV. The fraction of low-energy ions does not exceed 15–20%. The energy spectrum of an ion beam is determined by the shape of the accelerating voltage pulse. In the TEMP-4M accelerator, we use a Blumlein-nanosecond voltage pulse generator to form a voltage pulse of nanosecond duration. When the impedance of the Blumlein is matched with the load, a voltage pulse of a rectangular-like shape is applied to the load. In such a case, the content of low-energy ions in the beam is low.

Faraday cups

An essential element of the time-of-flight diagnostics is a detector that records ions and measures the ion current. The correctness of its operation largely determines the correctness of the entire diagnostics. To effectively transport and focus the HIPIB, it is necessary to ensure its ion space-charge compensation by low-energy electrons. Otherwise, due to Coulomb repulsion, the ion beam will be spilled.

For measuring the ion beam charge neutralization, we used a Faraday cup without magnetic field or voltage bias. This technique was used by Yatsui *et al.* (1985). The diameter of the collector was 8 mm, and the diameter of the hole in the lid was 4 mm.

https://doi.org/10.1017/S0263034618000186 Published online by Cambridge University Press

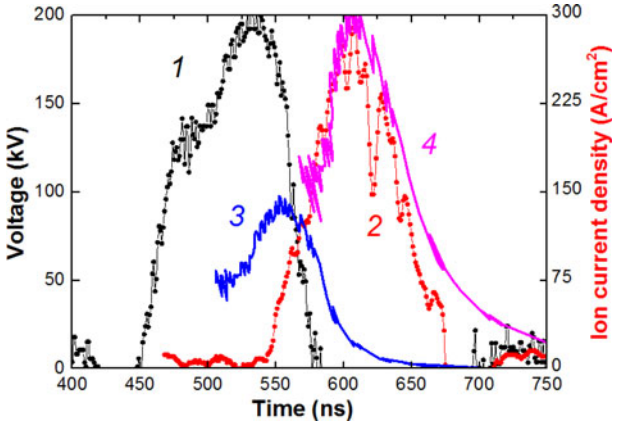


Fig. 12. Voltage waveforms, second pulse (1), ion current density (2, points) in a focusing diode, calculated current density of protons (3) and C^+ ions (4).

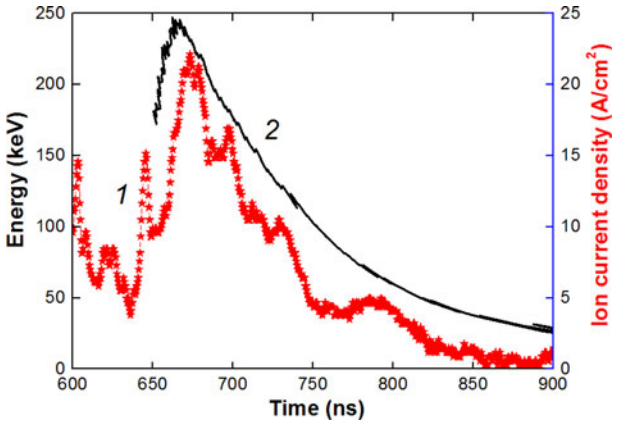


Fig. 13. Waveforms of the ion current density (1) and the kinetic energy of C^+ ions (2).

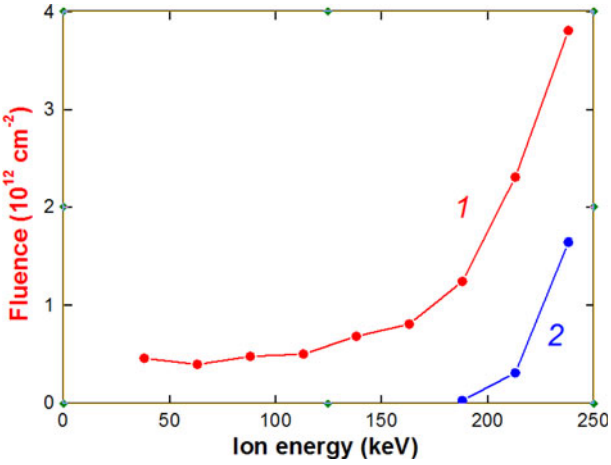


Fig. 14. The dependence of the fluence of C^+ ions (1) and protons (2) formed by the planar diode on their energy.

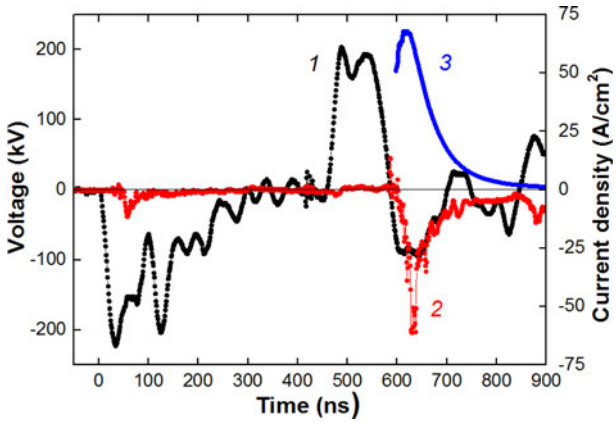


Fig. 15. Waveforms of the accelerating voltage (1), neutralized beam current density (2), and calculated current density of C^+ ions (3).

The Faraday cup was located at a distance of 14 cm downstream from the diode, in the focus. The Faraday cup is made of a BNC connector. Typical waveforms are shown in Figure 15.

The registration time of the neutralized beam current density agrees with the ion current density registration time, which confirms the correctness of measurement of HIPIB space charge.

However, when measuring the ion current density with a Faraday cup, these thermal low-energy electrons must be removed from the beam. For this purpose, a transverse magnetic field (CFC with magnetic cut-off) or a biased electric field (CFC with electric bias) is used. In this section, we present a comparative analysis of the techniques for measuring the parameters of an ion beam with the help of a CFC with a magnetic cut-off and a CFC with an electric bias.

CFC with magnetic cut-off

The Faraday cup is designed to measure the current density of charged particles. It is a collector for collecting the charge which is connected to a resistance, and has a collimating hole of a certain diameter, into which the investigated beam particles penetrate and hit the collector. Figure 16 shows a schematic illustration of the CFC structure.

Low-energy electrons that compensate the space charge of the beam ions are deflected in a magnetic field under and do not reach the collector of the CFC. The radius of motion of the electrons in the magnetic field (Larmor radius) is:

$$R_{\mathrm{L}} = \frac{m \times v}{e \times B} = \frac{\sqrt{2mE}}{e \times B}, \tag{8}$$

where $E = e \times U$ is the kinetic energy of an electron.

Figure 17 shows the dependence of the Larmor radius on the electron energy.

The energy of electrons that compensate the space charge of ions in the beam does not exceed 10 keV and the magnetic field created by a permanent magnet (0.2–0.3 T) is sufficient to prevent the electrons from entering the collector even with a small dimension of the CFC.

Previous studies (Pushkarev *et al.*, 2015b) showed that the skin layer of a neutralized ion beam generated by a diode with an accelerating voltage of 200–300 keV and a current density of more than 100 A/cm^2 is 2–3 mm. Therefore, the diameter of the collimating holes in the Faraday cup with magnetic cut-off can be 4–8 mm for effective removal of the low-energy electrons.

CFC with electric bias

To remove low-energy electrons from the ion beam, a bias electric field in the CFC can also be used. It has an additional metal plate

https://doi.org/10.1017/S0263034618000186 Published online by Cambridge University Press

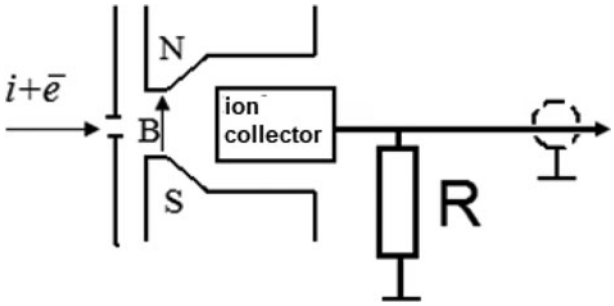


Fig. 16. Schematic illustration of the CFC with a transverse magnetic field.

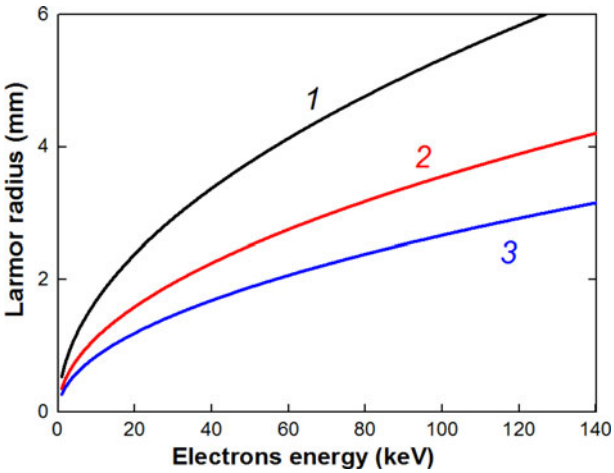


Fig. 17. Dependence of the Larmor radius on the electron energy at magnetic induction 0.2 T (1), 0.3 T (2), and 0.4 T (3).

with a collimating hole, at which a voltage of 300–500 V is applied. The polarity of the voltage can be any. Figure 18 shows a schematic illustration of the CFC with electric bias.

An ion beam, the ion charge in which is compensated by low-energy electrons, is a plasma object that effectively suppresses the penetration of an electric field into its volume. The distance covered by the action of an electric field in the plasma is determined by the Debye radius, which is (Reiser, 2008; Humphries, 1990)

$$\lambda_D = \sqrt{\frac{\varepsilon_0 \times k \times T}{n_e \times e^2}}, \quad (9)$$

where k is the Boltzmann constant and e is the electron charge.

For a HIPIB with singly ionized ions at full charge neutralization, $n_e = n_i$. Then the Debye radius, taking into account Eq. (8), is equal to:

$$\lambda_D = \sqrt{\frac{\varepsilon_0 kT \times e \times \sqrt{2U \times e}}{e^2 \times j \times \sqrt{m_i}}} = \sqrt{\frac{\sqrt{2} \times \varepsilon_0 kT}{\sqrt{e \times m_i}}} \times \frac{U^{1/4}}{\sqrt{j}}. \quad (10)$$

The Debye radius for HIPIB consisting of C^+ ions is:

$$\lambda_D = 0.3 \frac{U^{1/4}}{\sqrt{j}}, \ \mu m, \quad (11)$$

with the accelerating voltage in volts and ion current density in A/cm^2.

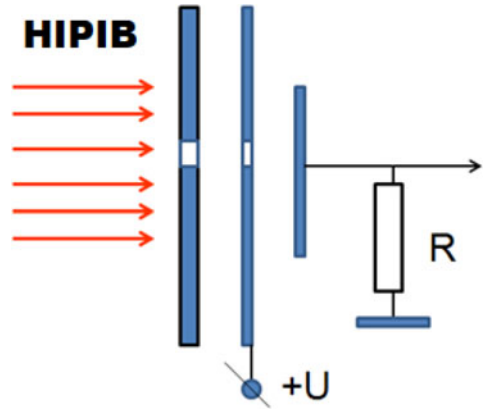


Fig. 18. Schematic illustration of the CFC with electric bias.

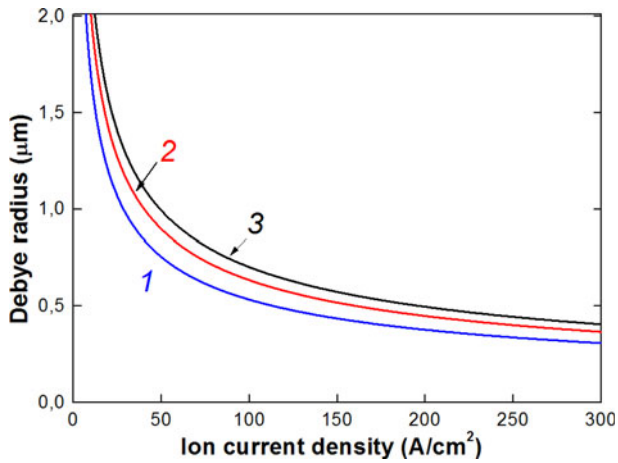


Fig. 19. Calculation of the Debye radius for low-energy electrons in HIPIB (T_e = 300 K) at an accelerating voltage of 100 kV (1), 200 kV (2), and 300 kV (3).

Figure 19 shows the calculation of the Debye radius for typical HIPIB parameters.

When using a Faraday cup with electric bias, the HIPIB diameter should be several microns, which at a current density of 30–150 A/cm^2 and a load resistance of 50 Ω provides a very weak signal. Therefore, in our experimental conditions, it is more promising to use a CFC with magnetic cut-off.

Conclusion

The developed time-of-flight diagnostics makes it possible to determine the main characteristics of HIPIBs: the composition of the beam (ion type and ionization rate), the absolute values of the ion current density, and the energy spectrum for each ion type with an accuracy of ±10%. The technique has been successfully tested on different ion accelerators, which form HIPIB of a complex composition at the energy level of 6–8 GW and the concentration of up to 2×10^{13} cm^{-3}.

We performed a comparative analysis of two types of CFCs with magnetic cut-off and with electric bias. When using a Faraday cup with electric bias, the HIPIB diameter should be a few microns to remove electrons, which at a current density of 30–100 A/cm^2 and a load resistance of 50 Ω provides a very weak signal. Therefore, it is more promising to use a CFC with magnetic cut-off of low-energy electrons.

https://doi.org/10.1017/S0263034618000186 Published online by Cambridge University Press

Acknowledgments. Data analysis and interpretation of experimental results were supported by Russian Science Foundation via grant no. 17-79-10140. The authors would like to thank Dalian University of Technology, especially Professors X. P. Zhu and M. K. Lei for support in maintaining experimental set-up, and in performing some of the experiments.

References

Aston FW (1920) Isotopes and atomic weights. *Nature* **105**, 617–619.

Bocharov GS, Eletskii AV, Zakharenkov AV, Zilova OS, Sliva AP, Terentyev EV, Fedorovich SD and Churilov GN (2018) Optimization of steel-surface hardening by carbon nanostructures followed by treatment with high-intensity energy sources. *Journal of Surface Investigation* **12**, 27–32.

Bystriskii VM and Didenko A (1989) *High Power Ion Beams*. New York: American Institute of Physics.

Cartwright BG, Shirk EK and Price PB (1978) A nuclear-track-recording polymer of unique sensitivity and resolution. *Nuclear Instruments and Methods* **153**, 457.

Davis HA, Bartsch RR, Olson JC, Rej DJ and Waganaar WJ (1997) Intense ion beam optimization and characterization with infrared imaging. *Journal of Applied Physics* **82**, 3223.

Fleischer RL, Price PB and Walker RM (1965) Ion explosion spike mechanism for formation of charged-particle tracks in solids. *Journal of Applied Physics* **36**, 3645.

Furman ÉG, Stepanov AV and Furman NZ (2007) Ionic diode. *Technical Physics* **52**, 621.

Ghadikolaee MRB and Ghadikolaee ET (2012) Design of a new faraday cup to measure the beam current of an ion source with residual gas. *Journal of Fusion Energy* **31**, 569–572.

Humphries S (1990) *Charged Particle Beams*. New York: Wiley, 847 p.

Isakova YI and Pushkarev AI (2018) Visualization and analysis of pulsed ion beam energy density profile with infrared imaging. *Infrared Physics and Technology* **89**, 140.

Kasuya K, Watanabe M, Ido D, Adachi T, Nishigori K, Ebine T, Okayama H, Funatsu M, Sunami H, Wu C, Hotta E and Miyamoto S (1999) Production, diagnostic and application of pulsed ion beams with light and medium mass. *Fusion Engineering and Design* **44**, 319–326.

Langmuir I (1913) The effect of space charge and residual gases on thermionic currents in high vacuum. *The Physical Review* **2**, 450.

Mamyrin BA (2001) Time-of-flight mass spectrometry (concepts, achievements, and prospects). *International Journal of Mass Spectrometry.* **206**, 251–266.

Moskalev VA (1992) *Measurement of the Parameters of Charged Particle Beams*. Moscow: Energoatomizdat.

Proskurovsky DI, Rotshtein VP, Ozur GE, Ivanov YF and Markov AB (2000) Physical foundations for surface treatment of materials with low energy, high current electron beams. *Surface and Coatings Technology* **125**, 49–56.

Pushkarev AI, Isakova YI and Khailov IP (2014) The effective anode-cathode gap in an ion diode operating in a bipolar-pulse regime. *Technical Physics Letters* **40**, 545.

Pushkarev AI, Isakova YI and Khailov IP (2015a) Intense ion beam generation in a diode with explosive emission cathode in self-magnetically insulated mode. *European Physical Journal D: Atomic, Molecular and Optical Physics* **69**:40.

Pushkarev AI, Isakova YI and Khailov IP (2015b) Analysis of correctness of intense ion beam diagnostics based on the ion-current density. *Instruments and Experimental Techniques* **58**, 667–674.

Reiser M (2008). *Theory and Design of Charged Particle Beams*. Wiley-VCH Verlag GmbH & Co. KGaA, 647 p.

Stephens WE (1946) A pulsed mass spectrometer with time dispersion. *The Physical Review* **69**, 691–692.

Wiley WC and MacLaren IH (1955) Time-of-flight spectrometer with improved resolution. *Review of Scientific Instruments* **26**, 1150–1157.

Xiao Y, Shen J, Qu M, Liu W, Zhong H, Zhang J, Zhang Y, Yan S, Zhang G, Zhang X and Le X (2015) Characterization and analysis of infrared imaging diagnostics for intense pulsed ion and electron beams. *Vacuum* **113**, 36.

Xin JP, Zhu XP and Lei MK (2011) On time-of-flight ion energy deposition into a metal target by high-intensity pulsed ion beam generated in bipolar-pulse mode. *Surface and Coatings Technology* **206**, 879–883.

Yatsui K, Tokuchi A, Tanaka H, Ishizuka H, Kawai A, Sai E, Masugata K, Ito M and Matsui M (1985) Geometric focusing of intense pulsed ion beams from racetrack type magnetically insulated diodes. *Laser and Particle Beams* **3**(Part 2), 119–155.

Yu X, Liu Z, Shen J, Isakova YI, Zhong H-W, Zhang J, Yan S, Zhang G-L, Zhang X-F and Le X-Y (2017) Dynamic energy spectrum and energy deposition in solid target by intense pulsed ion beams. *Nuclear Science and Techniques* **28**, 48.

Zhu XP, Dong ZH, Han XG, Xin JP and Lei MK (2007) Lifetime of anode polymer in magnetically insulated ion diodes for high-intensity pulsed ion beam generation. *Review of Scientific Instruments* **78**, 023301.

Zhu XP, Lei MK, Dong ZH and Ma TC (2003) Characterization of a high-intensity unipolar-mode pulsed ion source with improved magnetically insulated diode. *Review of Scientific Instruments* **74**, 47.

https://doi.org/10.1017/S0263034618000186 Published online by Cambridge University Press